Environmental Science
Processes & Impacts

Accepted Manuscript

ROYAL SOCIETY OF CHEMISTRY

rsc.li/process-impacts

Evaluating the applicability of a semi-continuous aerosol sampler to measure Asian dust particles

Se-Chang Son and Seung Shik Park*

Department of Environment and Energy Engineering, Chonnam National University, 77 Yongbong-Ro, Buk-ku, Gwangju 500-757, Korea

*Author to whom correspondences should be addressed: Tel: +82-62-530-1863 Fax: +82-62-530-1859; e-mail: park8162@chonnam.ac.kr

A Korean prototype semi-continuous aerosol sampler was applied to measure Asian dust particles. During two dust-storm periods, concentrations of crustal and trace elements were significantly enriched.

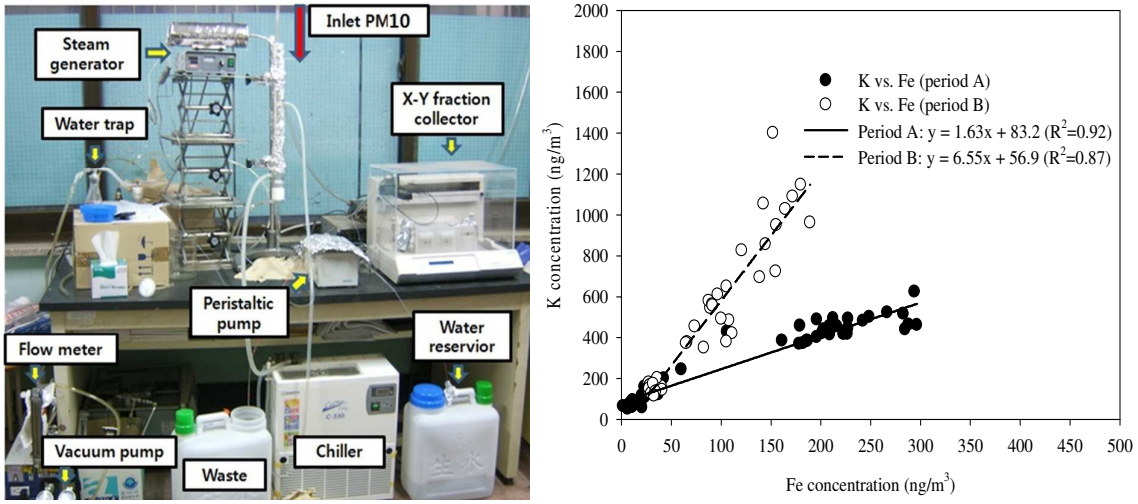

Abstract

Dust storm is one of the most important natural sources of air pollution in East Asia. The present study aimed to evaluate the applicability of a Korean Semi-continuous Aerosol Sampler (K-SAS) to observe the mineral dust particles during the dust storm events. Aerosol slurry samples were collected at 60-min intervals using the K-SAS, which is operated at a sampling flow rate of 16.7 l/min through a PM_{10} cyclone inlet. The measurements were done during dust storm events that occurred at an urban site, Gwangju in Korea, between April 30 and May 5, 2011. The K-SAS essentially utilizes particle growth technology as a means of collecting atmospheric aerosol particles. The concentrations of 16 elements (Al, Fe, Mn, Ca, K, Cu, Zn, Pb, Cd, Cr, Ti, V, Ni, Co, As, and Se) in the collected slurry samples were determined off-line by inductively coupled plasma-mass spectrometry (ICP-MS).

The sampling periods were classified into two types, based on the source regions of the dust storms and the transport pathways of the air masses reaching the sampling site. The first period "A" was associated with the dust particles that contain high Ca content and that originated from the Gobi desert regions of northern China and southern Mongolia. The second period "B" was associated with the dust particles originated in northeastern Chinese sandy deserts, which contain low Ca content. The measurement results from the K-SAS indicated that noticeable difference in concentrations of crustal and trace elements was found in the two sampling periods, due to the differences in the source regions of the dust storms, the air mass transport pathways, and the impact of the smokes of forest fires. The concentrations of the crustal (Al, Ca, Ti, Mn, and Fe) and anthropogenic trace elements (Vi, Ni, Cu, Zn, As, Se, and Pb) were significantly enriched during the two dust storm periods. However, the crustal elements were observed to be more enriched during dust storm period "A", while the concentrations of the trace elements were observed to be higher during period "B". Higher concentrations of K during dust storm period "B" could be ascribed to the smoke of forest fires, in addition to the soil dust emissions. This result can be supported by a strong correlation between the crustal elements and the K concentrations, the higher K/Al and K/Fe ratios in period "B" than those detected in the soil samples from the Gobi desert regions and Chinese sandy deserts, and the smoke from forest fires. The results of this study indicate that the K-SAS can be a good candidate for revealing the dynamics in the concentrations of elemental species in Asian dust particles, as well as in the urban and industrial aerosols, and for developing insight into their sources.

Keywords: Semi-continuous aerosol sampler, Asian dust particles, Elemental species, and Air mass transport pathway

Environmental impact

Results of this study suggest that a Korean semi-continuous aerosol sampler could be useful for revealing the dynamics in the concentrations of elemental species in Asian dust particles. The difference in the temporal behaviors of crustal and trace elements concentrations during the two dust-storm periods are likely the result of differences in the mineralogical composition of re-suspended soil materials, anthropogenic pollution sources, and probably the atmospheric processing of the aerosols.

Introduction

The Asian continent, where many deserts are distributed, is an important source region of dust emissions. Dust storms generated from these deserts travels rapidly over long distances,[1-7] causing a wide range of environmental problems such as poor air quality, adverse human health, and damages to animals, plants, crops, historical buildings, monuments and industrial activities.[8-11] In addition, the mineral dust particles affect the climate both directly by the scattering and absorption of solar radiation, and indirectly by acting as cloud condensation nuclei.[12-14] Moreover, it is though that mineral dust aerosols fall into the oceans during their long-range transport and significantly affect the oceanic ecosystem by regulating phytoplankton growth.[15,16] Previous studies have also shown that chemical concentrations of aerosols in dust storms observed in Asian region including China,[11,17-19] Taiwan,[20,21] Korea,[22,23] Japan,[17] and source regions[17] are significantly affected by the source area, size of dust storms, and the transport pathway.

Elemental species in ambient aerosol particles, which are derived from natural soil dusts and anthropogenic activities, have been employed for the tracing of emission sources[24-29] and for studies on health.[30-33] Highly time–resolved measurements of ambient aerosol particles can be used to enhance the understanding of the dynamic behaviors and sources of elemental species and to evaluate the exposures to short-term excursions, since the strength of the source emissions and the meteorological parameters vary on sub–hourly timescales.[24-28,34-37] Therefore, to provide improved temporal resolution of the elemental species concentrations in the ambient air particles, semi-continuous aerosol sampling systems have been developed. These systems include the Davis Rotating-drum Unit for Monitoring (DRUM),[38] the *S*emi-continuous Elements in Aerosol Sampler (SEAS),[39] and a Korean Semi-continuous Aerosol Sampler (K-SAS).[40] The systems perform sub-hourly or hourly collection of the ambient

aerosol particles for subsequent elemental analysis. An eight-stage DRUM sampler, with 3-hr time resolution and synchrotron X-ray fluorescence, was used to measure the size- and time-resolved concentrations of 19 elements during the spring of 2002 at Gosan, Korea, which is one of the representative background sites in East Asia.[35] The SEAS and K-SAS utilize particle condensation growth technology to collect ambient aerosol particles. However, the air sampling flow rate in the K-SAS is 16.7 l/min, which is approximately one fifth of the flow rate in the SEAS. Park *et al.*[37] compared 24-hr average elemental species concentrations from the hourly K-SAS samples with those derived from 24-hr integrated filter samples at an urban site. Strong correlations were observed between the concentrations of the elemental species measured by the two methods (mostly correlation coefficients (r) > 0.80). However, the concentrations of Al, K, Ca, Mn, and Fe were measured to be lower in the K-SAS samples than in the filter-based ones.

In an effort to reduce the large analytical time commitment for the semi-continuous sampling systems, online semi-continuous measurement systems have been developed and utilized for the rapid detection of the elemental composition of ambient aerosol particles. Examples of such online systems include Aerosol Time-of-Flight Mass Spectrometry (ATOFMS)[26,27] and the near-real time Xact field XRF analyzer (Cooper Environmental Services, Oregon, USA).[28,41,42]

In this study, hourly PM_{10} samples were collected at an urban site in Korea, downwind of China, for approximately four days using K-SAS, and used for subsequent elemental analysis by ICP-MS. The back-trajectories of the air masses arriving at the site were calculated to identify the probable source regions of the dust storms observed during the study period, and to examine the difference in the concentration ratios of maker elements in the dust particles.

Experimental

Collection of slurry samples

PM_{10} slurry samples were collected with the time interval of 60 minutes between 12:00 on April 30 and 10:00 on May 5, 2011, at an urban site (35°11′N, 126°54′E) in Gwangju, Korea, using the K-SAS developed by Lee *et al.*.[40] The sampling site was located on the rooftop of a three-story building at a university, approximately 100 m from a two-lane road carrying heavy traffic during rush hour, and significantly influenced by the dust and anthropogenic emissions from northern China.[7,23] During the measurement period, hourly temperature ranged from 8.7 to 25.1°C (average: 16.2°C) and relative humidity varied between 23% and 98% (average: 62%). The prevailing surface wind was typically westerly with wind speeds of 0.2-6.0 m/s.

The K-SAS system, which collects hourly ambient aerosol particle samples for elemental analysis, consists of a PM_{10} inlet, steam generator, condenser, air/droplet separator, and an X-Y fraction collector. Detailed descriptions and a schematic diagram of the K-SAS system are available.[37,40] The system utilizes the condensational growth of particles, similar to the principle of cloud formation. Ambient air is drawn through a PM_{10} inlet cyclone at a sampling flow rate of 16.7 l/min, mixed with saturated water vapor from the steam generator, and then grown in a condenser at 0.5°C. The grown particles in the condenser are directed to the air/droplet separator (the "aerosol impactor") and are separated as droplets from the airstream in the separator. A major feature of the K-SAS system is that a virtual impactor is not needed because of the low sampling flow rate of the air. The resulting droplets are transferred to an X-Y fraction collector (Gilson FC204, USA) with a multichannel peristaltic pump (Ismatec IPC-N-16) for storage in clean polypropylene vials (15 mL), every 1-hr. Lee *et al.*[40] have indicated that the collection efficiency of the grown particles in the aerosol impactor

determined by using mono-dispersed fluorescent polystyrene latex (PSL) particles (0.075, 0.2, 0.43, 0.92, 1.0, 1.9, and 4.8 μm) was 54.8±2.5, 56.0±0.6, 55.4±0.6, 61.4±0.8, 77.3±0.7, 79.1±0.5, and 99.0±1.0%, respectively. The lower efficiency for the smaller particles could be ascribed to be the incomplete growth of these particles. The overall collection efficiency of the 0.075 μm PSL particles for the entire K-SAS system (i.e., condenser, aerosol impactor, and transfer lines to the fraction collector) was 55%, with the condenser being the major source of particle loss, accounting for 31% of the input particles. Particle deposition in the sample outlet tube connected to the air pump was also significant, accounting for 11% of the input particles. Therefore further modification of the system is required to improve the collection efficiencies for particles < 1.0 μm.[40]

Prior to the sampling, the vials to collect the ambient samples and all the tools to be used were washed with 10% nitric acid, rinsed with ultrapure distilled de-ionized water (18.2 $M\Omega \cdot cm^{-1}$), which is produced by an ultrapure water purification system (Barnstead Nanopure, #D11901, Thermo Scientific, USA), and dried under laminar flow conditions. Within 24-hrs of collection, the samples were capped and kept in a freezer at -20°C until the elemental analysis was performed. Each vial was weighted before and after sampling to determine the volume of the collected samples.

Elemental analyses of slurry samples

The collected slurry samples were analyzed for 16 elemental species (Al, Fe, Mn, Ca, K, Cu, Zn, Pb, Cd, Cr, Ti, V, Ni, Co, As, and Se) by ICP-MS (Agilent Co., 7500ce, USA). 65% high-purity HNO_3 was added to each sample to be 2 % (v/v) acid concentration and the ultrasonic treatment of samples was conducted for 15 minutes. After sonication, the slurry samples were filtrated using a syringe membrane filter (Millipore 0.45 μm) to remove the insoluble particles

and then analyzed to determine the elemental species using ICP-MS. The combined effects of the acid (2.0 % v/v nitric acid) and the ultrasonic treatment improved the metals recovery and slurry stability.[40,43] All elemental concentrations were corrected for field blank values. In this study, the method detection limit (MDL) of an elemental species was calculated as the average blank value of the elemental species plus three times the standard deviation of the blanks. The MDL of Al, Fe, Mn, Ca, K, Cu, Zn, Pb, Cd, Cr, Ti, V, Ni, Co, As, and Se for the K-SAS measurements were 2.40 (absolute mass: 2.33 ng), 2.50 (2.43 ng), 0.55 (0.53 ng), 0.86 (0.83 ng), 0.99 (0.96 ng), 0.36 (0.35 ng), 0.71 (0.69 ng), 0.39 (0.38 ng), 0.01 (0.01 ng), 0.03 (0.03 ng), 0.10 (0.10 ng), 0.07 (0.07 ng), 0.05 (0.05 ng), 0.01 (0.01 ng), 0.03 (0.03 ng), and 0.32 (0.31 ng) ng/m^3, respectively. The measurement precision of the elemental species, defined as its relative standard deviation, showed significant differences with varying the concentrations of the elemental species studied, but indicated values of <20% for all the elements. The precision for Al, As, Cd, Ca, Cr, Co, Cu, Fe, Pb, Mn, Ni, K, Se, Ti, V, and Zn was 8.8, 3.6, 2.4, 3.2, 10.2, 20.1, 5.5, 8.4, 8.7, 8.5, 9.6, 9.0, 3.5, 8.5, 4.8, and 8.9%, respectively. The quality assurance of the analysis was also tested by NIST standard reference material (SRM) 1640a (Trace Elements in Natural Water) (See Table 1). The average recoveries of SRMs were compared with their reported values and approximately 100%±10% was recovered for the following elements: Al, As, Cd, Cr, Co, Cu, Fe, Pb, Mn, Ni, Se, V, and Zn.

In our previous study, a comparison of 24-hr average elemental species (Al, K, Ca, Mn, Fe, V, Cd, Zn, As, and Pb) concentrations determined from hourly K-SAS samples with those derived from 24-hr filter-based samples indicated good to excellent correlation coefficients, ranging from 0.76 for K to 0.99 for Al,[37] but regression slopes varied greatly with the elements studied. The concentrations of the crustal elements Al, K, Ca, Mn, and Fe were

lower in the K-SAS method (1.4 for K - 11.0 for Al times lower) than in the conventional filter-based method. This discrepancy could be attributed to the difficulties of transferring the insoluble dust particles to the collection vials in the K-SAS.[37,40] A similar result was also found in the SEAS.[25] Conversely, comparable results were found between the two methods for the trace elements studied (Zn, As, Cd, V, and Pb). Ratios of the concentrations measured by the two methods were within 2 except for Al and Fe. Therefore, it is anticipated that the concentrations of the major crustal elements (Al and Fe) with the exception of K and Ca, which were measured by the K-SAS in this study, were substantially underestimated compared with their actual concentrations.

Results and Discussion

Classification of sampling periods

Fig. 1 shows the temporal profiles of the hourly PM_{10} and its concentrations of the elemental species observed for the study period. The elemental species data observed between 12:00 on May 2 and 12:00 on May 3 were excluded, as the K-SAS malfunctioned and the dust particles that had been deposited at the bottom of both the condenser and the aerosol impactor had to be washed out. Hourly SO_2 concentration in Fig. 1 was observed using a SO_2 monitor (U.V. fluorescence method) from the Ministry of the Environment at a location about 1.5 km from our sampling site. The Korean Meteorological Agency reported that the dust storm events from China occurred between May 1 and May 4, 2011, in the Korean Peninsula. As shown in Fig. 1, on May 1, the PM_{10} concentration began to increase at 05:00, reaching a maximum concentration of 625 $\mu g/m^3$ at 13:00, before decreasing to 270 $\mu g/m^3$ at 00:00 on May 2. Afterwards, the PM_{10} concentration rose and declined repeatedly, and remained high until the morning of May 4 when the dust-storm events disappeared. To identify the source

regions of the dust storms observed during the study period, 4-day backward air trajectories were calculated for three altitudes (500, 1000, and 1500 m above ground level) by using the HYSPLIT model.[44] In this study, two dust storm periods were classified based on the transport pathways of the air mass reaching the study area. Periods "A" and "B" cover the time intervals of 13:00 on April 30 – 12:00 on May 2 (period "A") and 13:00 on May 3 – 09:00 on May 5 (period "B"), respectively. Fig. 2 shows the transport pathways of the air mass for period "A" (0000 UTC 01 May) and period "B" (1500 UTC 03 May 3). The air masses for the two periods were transported to the site along slightly different pathways. During period "A", dust storms originating in the Gobi desert regions of southern Mongolia and northern China passed through the Beijing and Tianjin regions of northern China before arriving at the sampling site. For period "B", the dust storms originating in the sandy deserts and loess located in the northeastern Inner Mongolia Plateau (i.e., the Hulun Buir, Horqin, and Hunshandake sand fields) passed over Shenyang region before reaching the sampling site. In addition, the MODIS image (http://earthdata.nasa.gov/firms) (Fig. 2(c)) and the transport pathway of the air mass suggest that the site during period "B" was likely influenced by the forest fires emissions, which had occurred at the borders between northern Mongolia and southern Russia. Consequently, the transport pathways of the air masses (Fig. 2) and MODIS image suggest that period "A" was characterized by aerosols derived from both the dust emissions from the Gobi deserts and from regional pollution. However, the aerosol samples collected during period "B" could be likely attributed to the emissions from the northeastern Chinese sandy deserts, regionally produced pollution, and forest fire emissions.

General characteristics of hourly elemental species concentrations

The concentrations of the 16 elemental constituents in PM_{10} for the two dust storm periods "A"

and "B" are summarized in Table 2. Previous literatures on the elemental composition of TSP and PM_{10} measured during the Asian dust storms in East Asia regions are also summarized, as shown in Table 3. Although the sampling methods and periods were not identical among the measurement sites, an overall view of elemental composition of aerosols in dust storms could be gained from the inter-site comparisons. As shown in Table 3, the concentrations of elemental species in PM_{10} in this study were much lower than those at upwind locations of our sampling site. In particular, a comparison of concentrations of crustal elements (Al, Ti, and Fe) observed in Yellow Sea and East China Sea[19] with those in the present study indicates that the concentrations of the major crustal elements (Al and Fe), which were measured by the K-SAS, were quite underestimated, requiring further modification of the system to improve the collection efficiencies of major crustal elements. However, higher concentration of Zn in this study may reflect the differences in the source strengths for air pollution. Finally, this comparison indicates that source region, strength of dust storms and transport pathway are important factors affecting the elemental compositions of dust storms observed at downwind locations.

As shown in Fig. 1 and Table 2, the concentrations of the crustal elements (Al, Ca, Ti, Mn, and Fe) were higher during period "A", whereas the concentrations of trace elements were observed to be higher during period "B". The opposite result was observed for K, which is an important element in soil dusts. The K concentration was observed to be lower in period "A" (average: 309 ng/m^3, range: 50-623 ng/m^3) than that during period "B" (average: 526 ng/m^3, range: 115-1400 ng/m^3). In particular, the concentration of Ca was much enhanced in period "A", ranging from 102 to 8991 ng/m^3 with an average of 4208 ng/m^3, compared with that during period "B" (average: 1641 ng/m^3, range: 524-4678 ng/m^3). Compared with the Al and Fe concentrations, the relatively elevated concentration of Ca was probably due to high

water-soluble Ca and low Ca loss in the transferring section of the K-SAS.[37] Some studies have indicated that the concentrations of water-soluble Na, Al, Fe, Ca, Mn, and Fe in the soil samples, which include Asian dusts and local Korean dusts, accounted for 0.6-2.7%, 0.03-0.15%, 0.7-3.6%, 3.3-6.5%, 0.2-1.0%, and 0.01-0.09% of their respective total concentrations.[6,45] A possible explanation for the significant difference in Ca between the two periods is given in detail below.

In addition, it was found that the concentrations of trace elements were also increased during the dust storm periods. The concentrations of K, Vi, Ni, Cu, Zn, Pb, As, and Se during period "B" were relatively enhanced compared with those during period "A". As discussed above, high concentrations of the primary crustal elements are likely a result of dust emissions. However, excess enhancements of anthropogenic elements, i.e., Vi, Ni, As and Se, were likely due to the air masses coming from polluted regions in northeast China, as shown in the transport pathways of the air masses. The enhancement of anthropogenic pollution elements has well been confirmed by previous studies,[7,18, 23,46,47] in which in addition to large amounts of crustal elements, dust storms carry significant quantities of anthropogenic aerosols over long distances. Strong correlations of V with Ni (R^2 of 0.74 and 0.71 (p values < 0.01) during periods "A" and "B", respectively) (not shown here) suggest the influence from oil combustion.[34] No significant difference in the As and Se concentrations was observed for the two periods. Concentrations of As and Se were 1.9±1.0 (0.2-4.6) and 2.3±1.1 (0.5-5.2) ng/m^3 for period "A", and 2.1±1.2 (0.3-4.8) and 3.3±2.1 (1.3-8.3) ng/m^3 for period "B", respectively. It has been demonstrated that Se and SO_2 can be used to identify coal combustion or coke emissions at receptor sites.[34,36] Moreover, an As/Se ratio of ~ 1.0 has been reported in air sheds influenced by coal combustion and used to distinguish between the influence of coal combustion and other anthropogenic sources.[28,36] Regression analysis between the As and Se

concentrations showed strong correlations with a slope of 0.78±0.25 and an R^2 of 0.73 (p value < 0.01) for period "A", and with a slope of 0.55±0.03 and an R^2 of 0.85 (p value < 0.01) for period B, suggesting their influence from similar sources. As shown in Fig. 1, when the concentrations of dust particles and their elemental species peaked simultaneously during periods "A" and "B", SO_2 also reached an almost maximum value, suggesting the increase of SO_2 concentration due to the long-range transport of the air masses. The maximum SO_2 concentrations for periods "A" and "B" were 10. 8 and 26.8 μg/m^3 at 09:00 on May 1 and 17:00 on May 3, respectively, which correlated well with the degree of enhancement in the concentrations of the anthropogenic elemental species. The SO_2 was also correlated with Se with R^2 of 0.52 and 0.69 (p value < 0.01) for periods "A" and "B", respectively, suggesting that As, Se and SO_2 could likely be attributed to similar emission sources. However, a low As/Se ratio (0.55) for period "B" suggests a likely influence of Se from additional anthropogenic emission sources, as well as from the coal-related industries. These results indicate that the two sampling periods differed noticeably in the concentrations of crustal and trace elements because of the differences in the source regions of the dust particles, the air mass transport pathways, and the impact of smoke from the forest fires.

Inferring possible sources of the observed K

As discussed in the previous section, although the strength of dust storms was weaker during period "B" than during period "A", the K concentration was approximately 1.5 times higher in period "B", suggesting that other emission sources, in addition to the dust storms, contributed to the observed K. The relationships of K with Al and Fe, which are representative elements of soil dusts, were investigated during the two periods (Fig. 3), to infer the probable sources for the K observed during period "B". If the excess K during the dust storm events is

associated with the dust storm, then a high degree of correlation between the crustal elements and K is expected. The concentration of K was strongly correlated with Al, Ca, Ti, Cr, Mn and Fe, with R^2 of 0.87, 0.84, 0.87, 0.86, and 0.92 (p values < 0.01) during period "A" and R^2 of 0.82, 0.77, 0.87, 0.84, 0.77, and 0.87 (p values < 0.01) during period "B", respectively. These results suggest that the K observed during the two periods "A" and "B" may clearly be associated with the dust storm. However, considerable differences in the slopes of K versus both Al and Fe (Fig. 3) were observed between periods "A" and "B". The K/Al and K/Fe ratios in the soil samples from China loess, Gobi deserts, and China sandy deserts were 0.07-0.18 and 0.08-0.50, respectively.[6,48] However previous studies have shown that the K/Al and K/Fe ratios in the biomass burning emissions are very high and vary significantly with the types of biomass materials burned. The K/Al and K/Fe ratios were 51.5-84.2 and 41.1-174.0 in emissions from the rice and wheat straws burning[49,50] and 77.8 and 54.9 in the burning emissions of woods (pine trees and spruces)[51], respectively. The K/Al and K/Fe ratios for period "A" were 0.74 and 1.63, respectively; these values are higher than in the source regions of the soil dust in China. The ratios for period "B" were 3.31 and 6.55, respectively, which are 4 to 5 times higher than those for period "A". Considering the correction factors of K/Al (0.13) and K/Fe (0.16), which are derived from the underestimation of K, Al, and Fe concentrations[37] in the K-SAS used in this work, the corrected K/Al and K/Fe ratios were 0.10 (=0.74×0.13) and 0.26 (=1.63×0.16) for period "A". These ratios are quite similar to those in the soil samples, indicating that these ratios could be responsible for the significant accumulation of insoluble dust particles in the aerosol impactor and in the transferring line to the collection vials of the K-SAS. The corrected ratios of K to Al and Fe for period "B" were 0.43 and 1.05, respectively; these are considerably greater than those in the soil samples, but relatively lower than those reported for the biomass burning aerosols. Considering

atmospheric dilution of biomass burning plumes during transport of air mass and high abundances of crustal elements (Al and Fe) in Asian dust particles, this result suggests that in addition to the soil dust emissions, other emission source (i.e., biomass burning), as confirmed by both the MODIS satellite observation (Fig. 2) and the higher K/Al and K/Fe ratios, could be responsible for the pronounced enhancement of K observed during the study period "B".

Investigation of the difference in Ca concentration between the two periods

As discussed in the previous section, the Ca concentration (compared to that of the other crustal elements) was extremely high during period "A", when the dust storm originated from the Gobi desert regions. Previous works have indicated that the noticeable differences in the chemical composition of the soil dusts that originated from different regions were derived from the amount of Ca, which depends on the types of dust.[5,48,52-54] For example, dust particles originated in the northern margin of the Tibetan Plateau, including the Gobi desert and its surrounding areas, are characterized by high contents of carbonate and dolomite, which are major contributors to the Ca. However the dolomite contents are relatively low in the dust particles originating from the sandy lands of Qtindag, Horqin, and Hulun Buir and their surrounding areas, and from the loess of the northeast China, compared with those from the Gobi deserts and Loess.[5] The Ca contents in the soils from the China loess and the Gobi desert areas are approximately 6-8 times greater than those in the soils from northeast sandy deserts. This suggests that although dust aerosols collected in eastern Asia and the western Pacific regions contain high amounts of Ca, the Ca contents in the dust aerosols could be used as an indicator to track the source regions of the dust samples. Previous studies have supported this hypothesis.[5,53,55-57] Therefore, this work confirms that the significant difference in the Ca concentrations between the two dust storm periods "A" and "B" can likely be

ascribed to the different source regions of the soil dusts, as well as to the severity of dust storms.

Summary and Conclusion

In this study, Asian dust particles were collected hourly for approximately 4 days at an urban site of Gwangju, Korea, downwind of the Asian continent. Subsequently, elemental analysis was conducted by ICP-MS to evaluate the applicability of the K-SAS to the dust storms. Two types of sampling periods were discerned, based on the transport pathway of the air mass arriving at the sampling site and the source regions of the dust storms. The first period "A" is associated with the dust particles from the Gobi desert and its surrounding areas, which contain high Ca content, and the second period "B" is associated with the dust particles from the northeastern Chinese sandy deserts, which, in comparison, have low Ca content.

It was shown that the concentrations of all the elemental species studied were relatively enhanced during the two periods in comparison with their background levels. The concentrations of the major crustal elements (Al, Ca, Ti, Mn, and Fe) were found to be higher during period "A", whereas the concentrations of the anthropogenic trace metals (V, Ni, Cu, Zn, As, Se, and Pb) were found to be higher during period "B". The dynamics in the concentrations of the crustal elements during the two dust-storm periods coincided with those of the trace elements, suggesting close association of their enrichment with the transport pathways of air masses passing over the polluted regions of northeastern China. The difference in the temporal behaviors of crustal and trace elements concentrations during the two periods are likely the result of differences in the mineralogical composition of re-suspended soil materials, anthropogenic pollution sources, and probably the atmospheric processing of the aerosols.

In contrast with the temporal profiles of the major crustal elements (Al, Ca, Mn, and Fe), higher concentrations of K were observed during period "B", suggesting some influence from the forest fire emissions in addition to the dust emissions, as supported by the higher K/Al and K/Fe ratios found in the dust particles collected for period "B" than those in Chinese soil dusts, and by the MODIS satellite image. Results from the study indicate that the Korean semi-continuous aerosol sampler could be useful for revealing the short-term variability in the concentrations of elemental species in Asian dust particles, as well as urban and industrial aerosols, and for developing insight into their sources.

Acknowledgement

This research was supported by Basic Science Research Program through the National Research Foundation of Korea (NRF) funded by the Ministry of Education (NRF-2014R1A1A4A01003896). Also authors wish to acknowledge a grant-in-aid for research from Gwangju Green Environment Center (14-2-40-41).

References

1 R.B. Husar et al., *J. Geophys. Res.*, 2001, **106**, 18317-18330.
2 T. Nakamura, K. Matsumoto and M. Uematsu, *Atmos. Environ.*, 2005, **39**, 1749–1758.
3 C.L. Heald et al., *J. Geophys. Res.*, 2006, 111, D14310, doi:10.1029/2005JD006847.
4 G. Roberts, G. Mauger, O. Hadley and V. Ramanathan, *J. Geophys. Res.*, 2006, **111**, D13205, doi:10.1029/2005JD006661.
5 G. Li, J. Chen, Y. Chen, J. Yang, J. Ji and L. Liu, *J. Geophys. Res.*, 2007, **111**, D17201, doi:10.1029/2007JD008676.
6 R.M. Duvall et al., *Atmos. Environ.*, 2008, **42**, 5872-5884.
7 S.S. Park and S.Y. Cho, *Aerosol Air Qual. Res.*, 2013, **13**, 1019-1033.
8 K. Kim, Y.J. Kim and S.J. Oh, *Atmos. Environ.*, 2001, **35**, 5157-5167.
9 B.K. Lee, H.K. Lee and N.Y. Jun, *Chemosphere*, 2006, **63**, 1106–1115.
10 R.J. Zhang et al., *Aerosol Air Qual. Res.*, 2010, **10**, 67–75.
11 J. Zhao, F. Zhang, Y. Xu, J. Chen, L. Yin, X. Shang and L. Xu, *Aerosol Air Qual. Res.*, 2011, **11**, 299–308.
12 R.A. Duce, Sources, distributions, and fluxes of dusts and their relationship to climate, in aerosol forcing of climate (Charlson, R.; Heintzenberg, J., Eds.), John Wiley: New Jersey, 1995.
13 S.E. Schwartz, *J. Aerosol Sci.*, 1996, **27**, 359-382.
14 S.K. Satheesh and K.K. Moorthy, *Atmos. Environ.*, 2005, **39**, 2089-2110.
15 J.K.B. Bishop, R.E. Davis and J.T. Sherman, *Science*, 2002, **298**, 817–821.
16 A. Tsuda et al., *Science*, 2003, **300**, 958–961.
17 I. Mori, M. Nishikawa, T. Tanimura and H. Quan, *Atmos. Environ.*, 2003, **37**, 4253-4263.

18 Y. Sun, G. Zhuang, Y. Wang, X. Zhao, J. Li, Z. Wang and Z. An, *J. Geophys. Res.*, 2005, **110**, D24209.
19 R. Zhao, B. Han, B. Lu, N. Zhang, L. Zhu and Z. Bai, *Atmos. Pollut. Res.*, 2014, Article in Press, doi: 10.5094/APR.2015.023.
20 M.-T. Cheng et al., *J. Atmos. Chem.*, 2008, **61**, 155-173.
21 J.-H. Tsai et al., *Aerosol Air Qual. Res.*, 2012, **12**, 1105-1115.
22 K.H. Kim, G.H. Choi, C.H. Kang, J.H. Lee, J.Y. Kim, Y.H. Youn and S.R. Lee, *Atmos. Environ.*, 2003,**37**, 753–765.
23 S.S. Park, Y.J. Kim, S.Y. Cho and S.J. Kim, *J. Air & Waste Manage. Assoc.*, 2007, 57, 434–443.
24 C.B. Kidwell and J.M. Ondov, *Aerosol Sci. Technol.*, 2004, **38**, 1-14.
25 J.P. Pancras, J.M. Ondov, N. Poor, M.S. Landis and R.K. Stevens, *Atmos. Environ.*, 2006, **40**, S467-S481.
26 B. de Foy, A.M. Smyth, S.L. Thompson, D.S. Gross, M.R. Olson, N. Sager and J.J. Schauer, *Atmos. Environ.*, 2012, **59**, 294-301.
27 A.M. Smyth et al., *Atmos. Environ.*, 2013, **73**, 124-130.
28 S.S. Park et al., *Atmos. Pollut. Res.*, 2014, **5**, 119-128.
29 S.M. Yi and I. Hwang, *Asian J. Atmos. Environ.*, 2014, **8**, 115-125.
30 J.D. Carter, A.J. Gjop, J.M. Samet and R.B. Devlin, *Toxicology and Applied Pharmacology*, 1997, **46**, 180-188.
31 H. Prieditis and I.Y. Adamson, *Experimental Lung Res.*, 2002, **28**, 563-576.
32 F. Schaumann et al., *American J. Respiratory Critical Care Med.*, 2004, **170**, 898-903.
33 K. Cheung, M.M. Shafer, J.J. Schauer and C. Sioutas, *Environ. Sci. Technol.*, 2012, **46**, 3779-3787.
34 D. Ogulei, P.K. Hopke, L. Zhou, P. Paatero, S.S. Park, S.S. and J.M. Ondov, *Atmos. Environ.*, 2005, **39**, 3751-3762.
35 J.S. Han et al., *Atmos. Chem. Phys.*, 2006, **6**, 211-223.
36 S.S. Park, J.P. Pancras, J.M. Ondov and A. Robinson, *Aerosol Sci. Technol.*, 2006, **40**, 883-897.
37 S.S. Park, J.M. Ko and D.S. Lee, *J. Korean Soc. Atmos. Environ.*, 2012, **28**, 39-51. (in Korean)
38 T.A. Cahill, C. Goodart, J.W. Nelson, R.A. Eldred, J.S. Nasstrom and P.J. Feeny, Design and evaluation of the DRUM impactor. *Proceedings of the International Symposium on Particulate and Multi-Phase Processes* (vol. 2) (Ariman, T. and Nejat, T., Eds), Taylor and Francis, Philadelphia, pp. 319–325, 1985.
39 C.B. Kidwell and J.M. Ondov, *Aerosol Sci. Technol.*, 2001, **35**, 596-601.
40 D.S. Lee, B. Lee and J.W. Eom, *Atmos. Pollut. Res.*, 2011, **2**, 506-512.
41 V. Yadav, J. Turner, K. Petterson and J. Cooper, Field performance evaluation of the Cooper Environmental Services ambient metals monitor (Xact 620) for near-real time PM_{10} metals monitoring. *Proceedings of 29th American Association for Aerosol Research Annual Conference*, October 28, 2010.
42 S.S. Park, S.A. Jung, B.J. Gong, S.Y. Cho and S.J. Lee, *Aerosol Air Qual. Res.*, 2013, **13**, 957-976.
43 J.P. Pancras, J.M. Ondov and R. Zeisler, *Anal. Chimica Acta*, 2005, **538**, 303–312.
44 R.R. Draxler and G.D. Rolph, HYSPLIT (HYbrid Single-Particle Lagrangian Integrated Trajectory) Model access via NOAA ARL READY Website (http://ready.arl.noaa.gov/HYSPLIT.php). NOAA Air Resources Laboratory, Silver Spring, MD, 2014.

45 S.Y. Sim, S.S. Park, D.R. Kim and S.J. Lee, *J. Korean Soc. Atmos. Environ.*, 2013, **29**, 64-73. (in Korean)
46 R. Arimoto, R.A. Duce, D.L. Savoie, J.M. Prospero, R. Talbot, J.D. Cullen, U. Tomza, N.F. Lewis and B.J. Ray, *J. Geophys. Res.*, 1996, **101**, 2011-2023.
47 J.H. Guo, K.A. Rahn and G.S. Zhuang, *Atmos. Environ.*, 2004, **38**, 855-862.
48 J.-S. Han et al., *Environ. Impact Assess.*, 2004, **13**, 277-284. (in Korean)
49 S.Q. Turn et al., *J. Geophys. Res.*, 1997, **102**, 3683-3699.
50 H.S. Lee, C.-M. Kang, B.-W. Kang and S.-K. Lee, *J. Korean Soc. Atmos. Environ.*, 2004, **20**(3), 317-330. (in Korean)
51 J.G. Watson, J.C. Chow and J.E. Houck, *Chemosphere*, 2001, **43**, 1141-1151.
52 J. Li and J. Zhang, *Mar. Geol. Quaternary Geol.*, 2003, **23**, 43–49.
53 X. Wang, D. Xia, T. Wang, X. Xue and J. Li, *Geomorphology*, 2008, **97**, 583–600.
54 D.-R. Kim, J.-S. Kim and S.-J. Ban, *J. Korean Soc. Atmos. Environ.*, 2010, **26**, 606-615. (in Korean with English abstract)
55 T. Zhang and X. Dong, *Environ. Monit. in China*, 2002, **18**, 11–14.
56 J.J. Cao et al., *J. Geophys. Res.*, 2005, **110**, D03203. doi:10.1029/2004JD005244.
57 Y.Q. Wang, X.Y. Zhang, R. Arimoto, J.J. Cao and Z.X. Shen, *Atmos. Environ.*, 2005, **39**, 2631–2642.

512
513 **Table 1** Results for analyses of SRM 1640a, trace elements in natural water

Element	Certified value (μg/L)	Measured value (μg/L)	Measured/Certified
Al	53.0±1.80	54.89±4.06	1.04±0.08
As	8.08±0.07	8.37±0.67	1.04±0.08
Cd	3.99±0.07	4.36±0.33	1.09±0.08
Cr	40.54±0.30	40.24±1.17	0.99±0.03
Co	20.24±0.24	20.23±0.77	1.00±0.04
Cu	85.75±0.51	88.25±2.90	1.03±0.03
Fe	36.8±1.80	37.51±2.62	1.02±0.07
Pb	12.10±0.05	12.76±0.56	1.05±0.05
Mn	40.39±0.36	40.63±2.24	1.00±0.06
Ni	25.32±0.14	25.50±1.42	1.01±0.06
Se	20.13±0.17	22.13±1.79	1.10±0.09
V	15.05±0.25	15.75±0.41	1.05±0.03
Zn	55.64±0.35	56.86±3.06	1.02±0.06

514
515
516
517
518
519

520
521 **Table 2** Summary of elemental species concentration over the study period (unit: ng/m^3)

Species	Period A		Period B	
	Average	Range	Average	Range
Al	291	10-657	134	33-323
K	309	50-623	526	115-1400
Ca	4208	102-8991	1641	524-4678
Ti	3.3	0.3-6.6	2.1	0.2-5.8
V	2.9	0.4-5.5	3.9	0.2-9.2
Cr	0.6	0.1-1.2	0.9	0.3-2.0
Mn	44	2-100	28	8-91
Fe	139	2-296	89	27-189
Co	0.3	0.0-0.8	0.2	0.0-0.4
Ni	1.6	0.5-3.1	2.7	1.0-5.3
Cu	3.6	1.4-9.1	6.9	2.7-19.9
Zn	80	24-159	407	49-1632
As	1.9	0.2-4.6	2.1	0.3-4.8
Se	2.3	0.5-5.2	3.3	1.3-8.3
Cd	0.5	0.0-1.4	0.8	0.2-1.8
Pb	19.0	3.7-40.3	29.5	7.9-79.4

522
523

524 **Table 3** A comparison of mass (μg/m^3) and elemental concentrations (ng/m^3) of aerosols during Asian dust storms in East Asia

Site	China Zhagjiakou[1)]	China Beijing[1)]	Japan Yamaguchi[1)]	Korea Seoul[2)]	China Beijing[3)]	China Beijing[3)]	Taiwan Taichung[4)]	Taiwan Pintung[5)]	China Xiamen[6)]	Yellow Sea[7)]	East China Sea[7)]	This Study[8)]	This Study[9)]
TSP	4500	1500	200	-	2497	2121	-	-	843	-	-	-	-
PM_{10}				144	-	-	175	55.4	-	87.3	59.0	200	129
Al	183000	95000	16000	4790	151000	146000	5936	741	21836	4438	6780	291	134
K	54000	28000	6000	1712	-	-	2920	516	1744	-	-	309	526
Ca	66900	43600	10300	3916	178000	58000	5555	1069	-	4237	3218	4208	1641
Ti	12100	6100	1100	223	10000	8800	304	3.6	351	224	367	3.3	2.1
V	254	130	33	28	260	220	-	-	41	38	18	2.9	3.9
Cr	-	-	-	20	230	140	-	3.6	23	-	-	0.6	0.9
Mn	2250	1210	210	156	1370	1330	126	10	612	23	17	44	28
Fe	98000	51000	9000	3960	89000	80000	3612	521	19278	1819	2751	139	89
Co	52	26	5.0	5.4	58	37	-	-	9.2	-	-	0.3	0.2
Ni	103	51	16	70	13	20	-	8.2	17	34	16	1.6	2.7
Cu	-	-	-	53	100	170	39	8.3	-	20	21	3.6	6.9
Zn	372	274	309	372	310	280	377	14	327	122	110	80	407
As	-	-	-	-	120	37	14	-	19	15	14	1.9	2.1
Se	-	-	-	-	-	-	-	-	-	-	-	2.3	3.3
Cd	-	-	-	7.7	5.8	3.0	7.0	0.1	-	-	-	0.5	0.8
Pb	207	46	173	133	260	160	229	4.9	475	34	21	19	30

525 Note)[1)]Mori et al. (2003)[17], period: March 2001, [2)]Kim et al. (2003)[22], period: March – May, 2001, [3)]Sun et al. (2005)[18], period: Spring 2002, [4)]Cheng et al. (2008)[20], period:
526 November 29, 2005, [5)]Tsai et al. (2012)[21], period: March 21-22, 2010, [6)]Zhao et al. (2011)[11], period: March 21-22, 2010, [7)]Zhao et al. (2014)[19], period: March-April, 2011, [8)]
527 This study "A" period: 13:00 on April 30 – 12:00 on May 2, 2011, [9)]This study "B" period: 13:00 on May 3 – 09:00 on May 5, 2011
528
529

530
531
532

A List of Figure Captions

534 Fig. 1 Temporal profiles of PM_{10} and its elemental species concentrations

535 Fig. 2 Back trajectories of the air mass arriving at the site for the two periods "A" (A) and "B"
536 (B), and the MODIS satellite image (C). The symbols in trajectories; △: 500 m AGL,
537 □: 1000 m AGL, ○: 1500 m AGL

538 Fig. 3 Relationship of K with the Al and Fe concentrations during the two dust storm periods

539

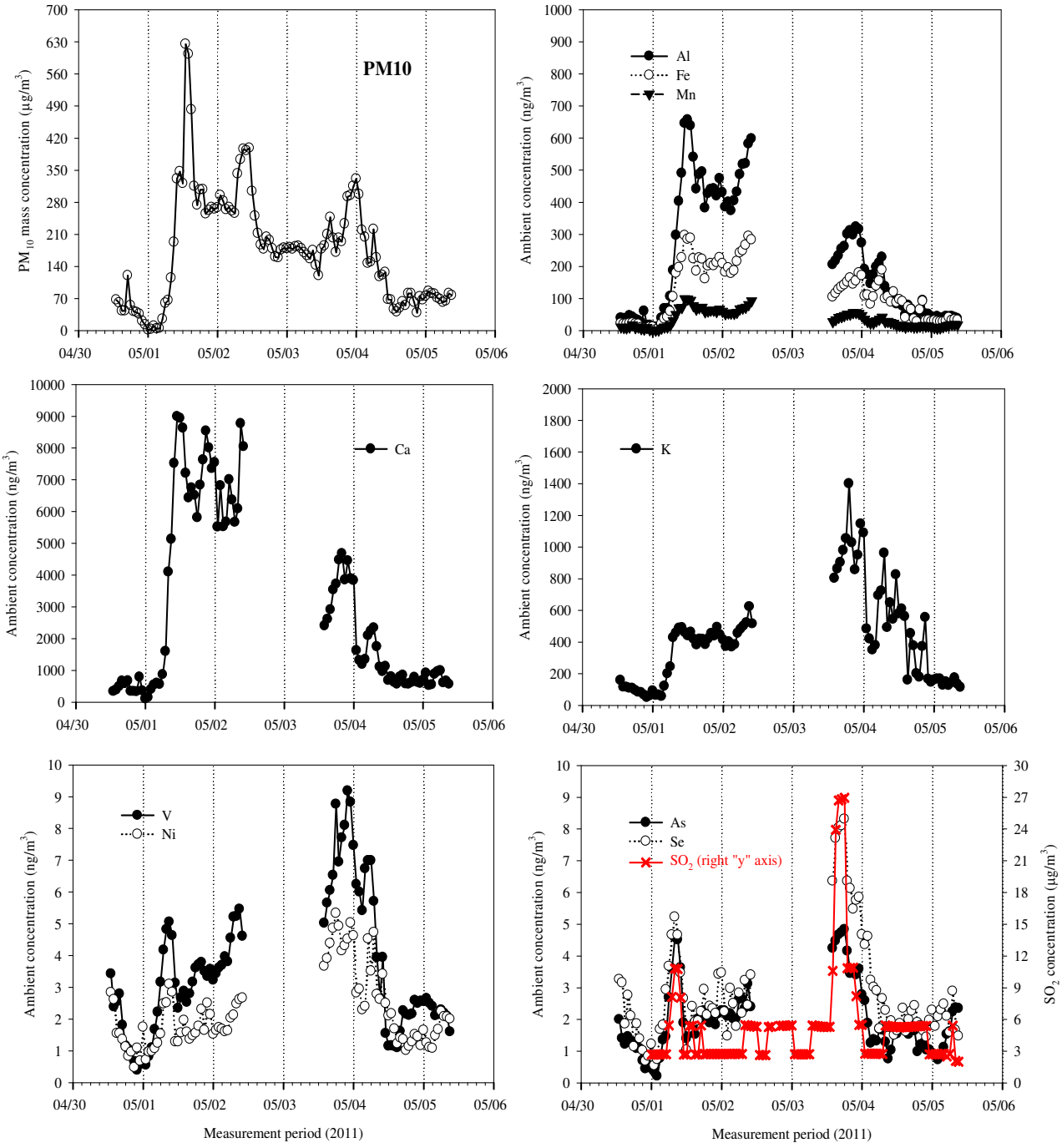

Fig. 1. Temporal profiles of PM_{10} and its elemental species concentrations

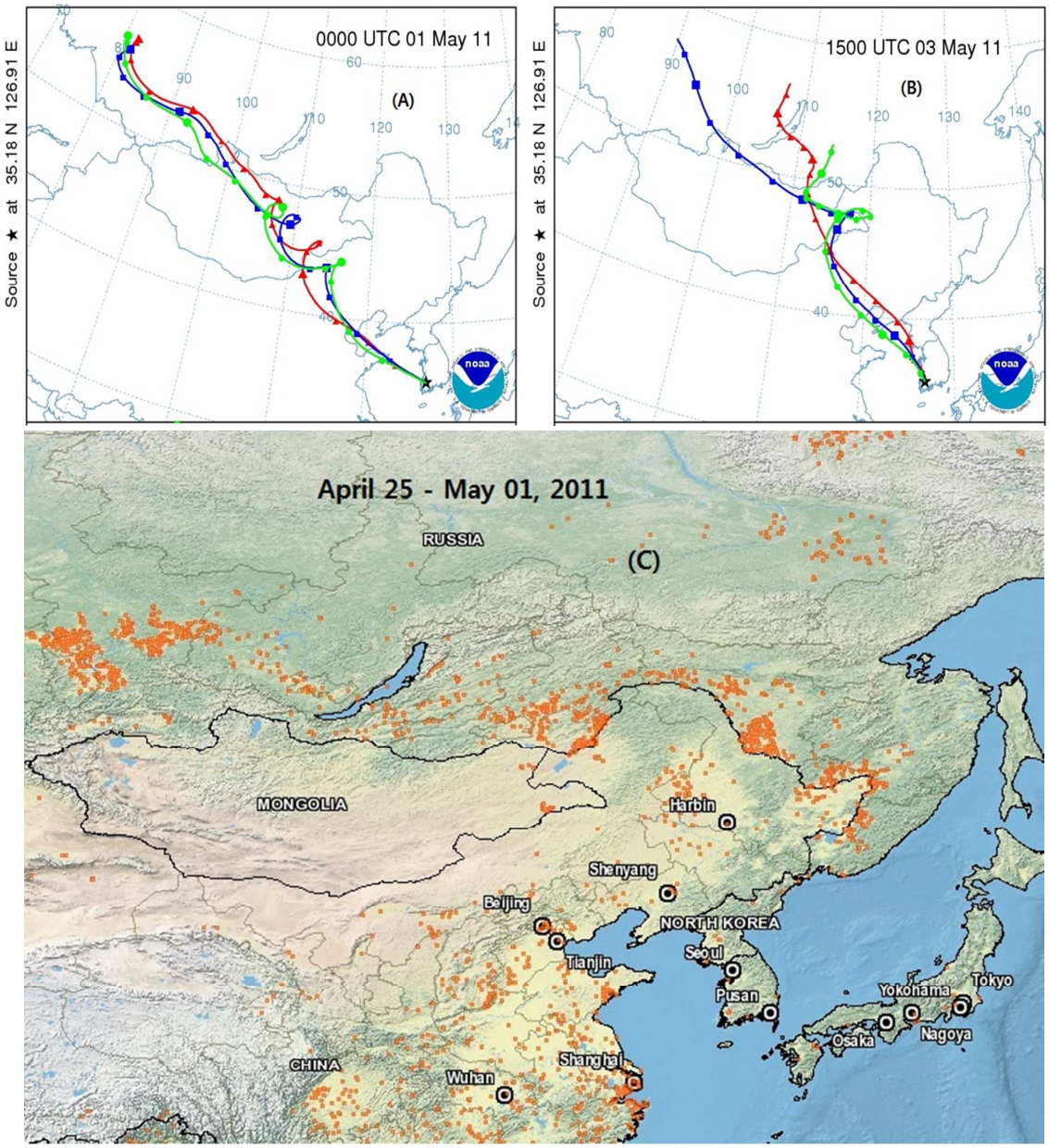

Fig. 2. Back trajectories of the air mass arriving at the site for the two periods "A" (A) and "B" (B), and the MODIS satellite image (C). The symbols in trajectories; △: 500 m AGL, □: 1000 m AGL, ○: 1500 m AGL

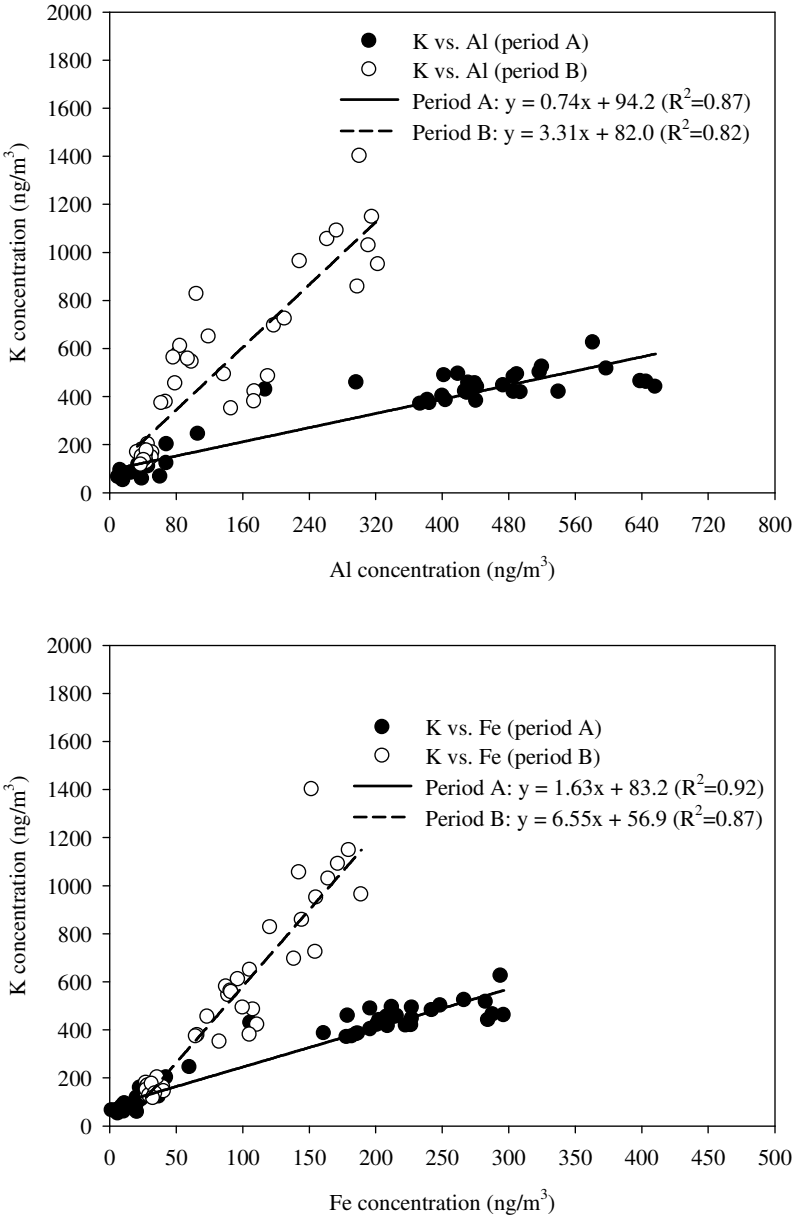

Fig. 3. Relationship of K with the Al and Fe concentrations during the two dust storm periods